DTIC
SELECTED
OCT 1 4 1994
F

surface science

A surface spectroscopic study of ultra-thin Ni films on Mo(110)

Jian-Wei He, W. Kevin Kuhn [1] and D. Wayne Goodman [2]

Department of Chemistry, Texas A&M University, College Station, TX 77843-3255, USA

The morphology, structures and CO chemisorptive properties of ultra-thin Ni films on a Mo(110) surface have been studied using Auger electron spectroscopy (AES), low energy electron diffraction (LEED), temperature programmed desorption (TPD), and infrared reflection absorption spectroscopy (IRAS). It is found that Ni grows layer-by-layer on Mo(110) at a sample temperature of 115 K; however, upon annealing to > 600 K, Ni multilayers form three-dimensional clusters. The Ni TPD spectra show two peaks corresponding to desorption from Ni 3D clusters and a 2D uniform monolayer, respectively. Two LEED structures, (8×2) and (7×2), are observed for Ni/No(110) and are attributed to Ni overlayers with distorted Ni(111) lattices. The (8×2) phase is found to transform to the (7×2) phase at a Ni coverage of ~ 1 monolayer. This phase transition is also observable in the CO IR spectra. CO adsorbed on the (8×2) and (7×2) Ni structures shows characteristic stretching frequencies at 2087 and 2065 cm^{-1}, respectively. In addition, the formation of the Ni(7×2) structure from disordered Ni is also reflected in the CO IR spectra. The enthalpy difference between the (7×2) and the disordered phases is determined to be 3.5 kcal/mol with the (7×2) phase being more stable. Upon the deposition of Ni onto CO/Mo(110) at 80 K, CO is found to spill-over from the Mo substrate onto the Ni overlayer resulting in a CO/Ni/Mo(110) structure. Finally, IR spectra of CO on Ni/Mo(110) surfaces as a function of CO coverage and annealing temperature are presented and discussed in terms of surface structure and CO mobility.

1. Introduction

Recently considerable scientific attention has been directed toward the study of bimetallic systems [1–11]. In these studies, the properties of metal–metal interfaces have been explored using a variety of surface science techniques. It has been shown that ultra-thin metal films usually have different structural, electronic and chemisorptive properties compared to those of the bulk metal surface [1–4]. For example, submonolayer Ni and Pd overlayers grow pseudomorphically on a W(110) substrate, i.e., they assume the substrate lattice rather than their typical bulk structures [2,3]. In addition, X-ray photoelectron spectroscopic (XPS) studies have shown that these metal monolayers are electronically perturbed relative to the surface atoms in the corresponding bulk metal [1]. Furthermore, CO

adsorbed onto bimetallic surfaces exhibits significant absorption energy changes compared to CO on the corresponding bulk metal surface [1–3].

In a recent study using Auger electron spectroscopy (AES), low energy diffraction (LEED) and work function measurements, it was reported that Ni forms two structures ((8×2) and (7×2)) on a Mo(110) surface at room temperature [9]. The (8×2) structure was found to transform into the (7×2) structure as Ni coverage increased from 0.74 to 1.29 monolayers (ML). This transition was shown to correlate with a work function increase of ~ 0.26 eV. An additional study has shown that the atoms in a monolayer of Ni on Mo(110) are significantly perturbed relative to the surface atoms of Ni(100) [10].

Recently, we have studied ultra-thin Ni films on a Mo(110) surface using AES, LEED, temperature programmed desorption (TPD), and infrared reflection absorption spectroscopy (IRAS). The results will be reported and discussed in this paper with the objective being to understand the morphological, structural and CO chemisorptive

[1] Present address: Frank J. Seiler Research Laboratory (FJSRL/NC), 2354 Vandenburg Dr., Suite 2A35, USAF Academy, CD 80840, USA.

[2] To whom correspondence should be addressed.

DTIC QUALITY

properties of ultra-thin Ni films. The understanding of the Ni–Mo bimetallic system is of practical importance since Ni–Mo bimetallics supported on alumina are used extensively as catalysts for hydro-desulfurization reactions [12].

2. Experimental

The experiments were carried out in two conventional ultra-high vacuum chambers. One was equipped for LEED, AES and TPD, and the other for IRAS, LEED and AES. These two systems have been described in detail previously [13,14]. The sample was spot-welded onto two 0.5 mm Ta wires which allowed resistive heating to 1500 K and cooling to 90 K. In addition, the sample could be heated to 2300 K using e-beam heating. A W/5%Re–W/26%Re thermocouple was spot-welded to the sample edge for temperature measurement.

The Mo(110) surface was cleaned using the procedure described in ref. [15]. Surface carbon was removed by repeated cycles of oxidation (1200 K, 10^{-7} Torr O_2) and annealing of the sample to 1900 K in vacuum. After this procedure, AES indicated a clean surface (atomic O, S, and C < 1%), and LEED exhibited a sharp substrate pattern with low background intensity.

The Ni deposition was performed by resistively heating a W filament wrapped with high purity Ni wire. Prior to each metal deposition, the source was degassed extensively. AES showed that less than one atomic percent C and O accumulated on the surface during the metal deposition.

Ni coverages were determined using Ni TPD area analysis and one Ni atom per substrate atom is defined as one monolayer (ML). All TPD spectra were acquired using a ~ 10 K/s heating ramp rate.

3. Results and discussion

3.1. AES of Ni on Mo(110)

Ni deposited onto a Mo(110) surface at a sample temperature (T_s) of 115 K was found to grow

layer-by-layer (the Frank–Van der Merwe mechanism). At temperatures > 600 K, multilayer Ni forms a uniform layer covered by three-dimensional (3D) clusters (Stranski–Krastanov (SK) mechanism). Fig. 1 shows the Ni(848 eV)/Mo(186 eV) AES ratio as a function of annealing temperature. The Ni was deposited onto the Mo(110) surface at 115 K and then annealed to the indicated temperatures. In fig. 1, the AES ratio at a Ni coverage (θ_{Ni}) of 0.95 ML is essentially unchanged upon annealing to ~ 800 K, indicating that during annealing, the submonolayer Ni remains as a uniform 2D layer. Fig. 1 also shows that annealing Ni multilayers to T_s > 600 K decreases the AES ratio considerably, indicating either the formation of 3D Ni clusters or alloying at the Ni–Mo interface [3,7–9]. As will be seen, the Ni TPD spectra show a peak characteristic of the sublimation from 3D Ni clusters discounting the possibility of alloying between the Ni multilayers and Mo substrate. The small increase in the Ni/Mo AES ratios at 320–600 K in fig. 1 is due to dispersion of small Ni 3D clusters into a
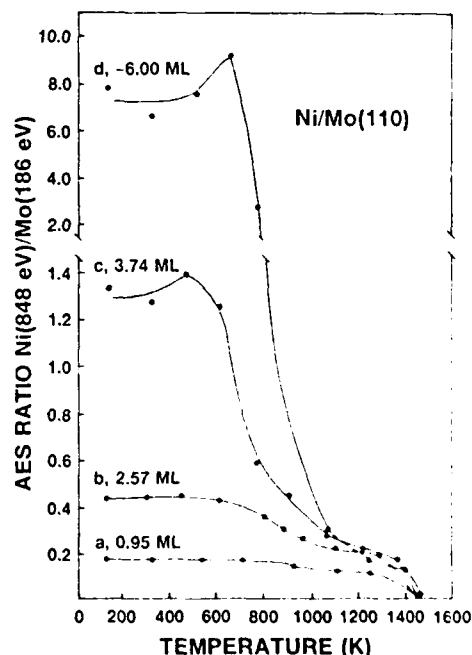

Fig. 1. The Ni(848 eV)/Mo(186 eV) AES ratios as a function of annealing temperature. The Ni was deposited onto the Mo(110) surface to the indicated coverages at 115 K.

2D film. The formation of small 3D clusters at 90 K and their dispersion at elevated temperatures are also indicated in the CO IR spectra.

3.2. TPD of Ni on Mo(110)

TPD spectra of Ni on Mo(110) are presented in fig. 2. Ni was deposited onto the Mo(110) surface at 115 K. Two desorption states in fig. 2 are evident and labeled β_1 and β_2 with the β_1 state showing a common leading edge characteristic of zero-order kinetics. Using an Arrhenius plot, the desorption activation energy (E_a) for the β_1 state is estimated to be 91 kcal/mol. This value agrees well with the bulk Ni sublimation energy of 94 kcal/mol [16]. The spectra in fig. 2 are typical for thin metal films in which the metal atoms form a uniform layer covered by 3D clusters (SK growth). The β_1 and β_2 states, therefore, correspond to desorption from 3D Ni clusters and the uniform Ni monolayer, respectively. Alloy formation between Ni and the Mo substrate is thus unlikely.

3.3. LEED structures of Ni on Mo(110)

The deposition of Ni at 115 K and subsequent annealing to ~ 500 K induces two LEED patterns. From 0.42 to 0.95 ML, an (8 × 2) structure

Fig. 3. (a) The schematic drawing of the (7 × 2) LEED pattern of Ni on a Mo(110) surface. The (7 × 2) structure of Ni/Mo(110) in real space. The open and filled circles represent Mo and Ni atoms, respectively.

is evident, and for $\theta_{Ni} \geq 1.08$ ML, a (7 × 2) structure appears. A schematic drawing of the (7 × 2) LEED pattern is shown in fig. 3a. Fig. 3b is a real space representation of the (7 × 2) structure. The open and filled circles represent Mo and Ni atoms, respectively. In fig. 3a, there are 6 satellite spots between two integral spots along the ⟨001⟩ direction. This pattern is assigned as (7 × 2) relative to the lattice parameters C_1 and C_2. For the (8 × 2) pattern, there are 7 satellite spots, instead of 6, between the two integral spots along the ⟨001⟩ direction. The (7 × 2) pattern remains visible even when multilayers (~ 6 ML) of Ni are present. These LEED results agree with previous work that also reported the (8 × 2) and (7 × 2) patterns and the structural phase transition at Ni coverages between 0.74 and 1.29 ML [9]. The (8 × 2) structure was, however, reported to be metastable and not observed by LEED for Ni deposition and LEED observation at 600 K [9].

Similar structures have been observed for Co/Mo(110) and Ni/W(110), where the overlayer atoms were interpreted to assume distorted Co(0001) and Ni(111) lattices, respectively [2,9]. The (8 × 2) and (7 × 2) Ni structures are, therefore, identified as corresponding to distorted
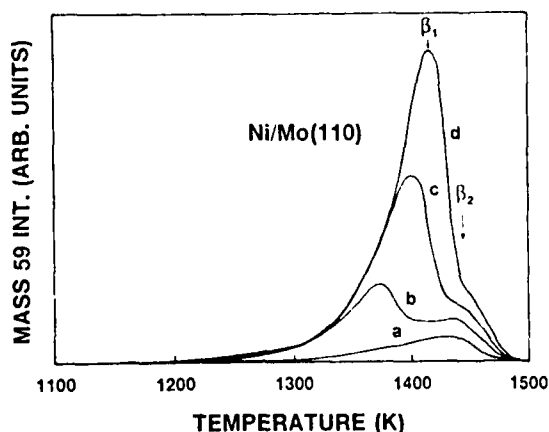

Fig. 2. Thermal desorption spectra of Ni from Mo(110). Ni was deposited onto the Mo(110) surface to the indicated coverages at 115 K: (a) 0.54 ML, (b) 2.37 ML, (c) 4.03 ML, and (d) 5.93 ML.
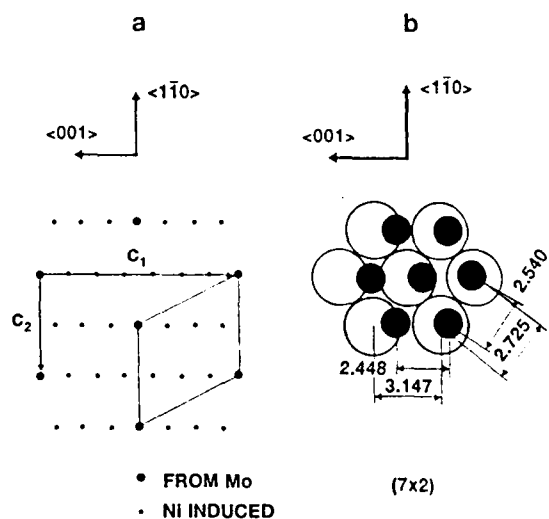
Ni(111) phases. The fractional spots are induced by electron beam double diffraction [17]. In real space (fig. 3b), the lattice of the Ni(7 × 2) structure matches that of the Mo(110) surface in the $\langle 1\bar{1}0 \rangle$ direction. In the $\langle 001 \rangle$ direction, however, every 9th Ni atom coincides with every 7th Mo atom. The lattice constants for the Ni(7 × 2) structure are calculated to be 2.448 and 2.540 Å, compared to 2.492 Å for a Ni(111) surface. Thus, the differences in the lattice constants between the Ni(7 × 2) structure and a Ni(111) surface are only 1.8% and 1.9%, respectively. The Ni(8 × 2) overlayer has a structure similar to the (7 × 2) but with lattice constants of 2.518 and 2.557 Å, respectively. The Ni coverages of the (8 × 2) and (7 × 2) structures on Mo(110) are 1.250 and 1.286 ML, respectively while the density of a Ni(111) surface corresponds to 1.303 ML. As will be seen, the (8 × 2) to (7 × 2) phase transition clearly correlates with an abrupt change in the CO IR spectra.

It is noteworthy that the (7 × 2) structure remains visible at Ni coverages as high as 5 ML. TPD and AES measurements, however, indicate the formation of 3D Ni clusters. Apparently, these 3D clusters grow epitaxially with the Ni(111) face parallel to the substrate surface, and the LEED spots from the 3D clusters overlap with those of the (7 × 2) structure.

3.4. TPD spectra of CO on Ni / Mo(110)

Fig. 4 shows the TPD spectra of CO from Ni/Mo(110) at the indicated Ni coverages. The Ni was deposited onto Mo(110) and then dosed with 20 L of CO at $T_s = 115$ K. At a Ni coverage of 1.0 ML, the CO desorption features from the Mo(110) substrate have been greatly diminished, while two new peaks (γ_1 and γ_2) at 380 and 825 K appear. For 3.05 ML of Ni, the γ_2 peak is no longer present, and the γ_1 peak has shifted to higher temperature. Using the Redhead approximation a frequency factor of 10^{13} and assuming first-order kinetics [18], the activation energies (E_a) for γ_1 and γ_2 are estimated to be 22.7 and 50.3 kcal/mol, respectively. The peak temperature of 420 K for the γ_1 state at $\theta_{Ni} = 3.05$ is close to that of CO from a Ni(111) surface (430
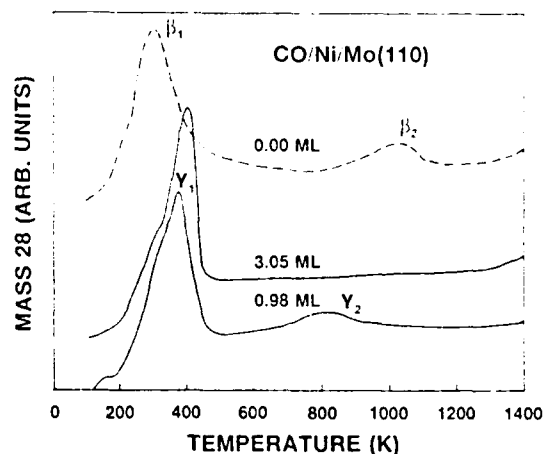

Fig. 4. Thermal desorption spectra of CO from Ni/Mo(110) surfaces. The Mo(110) was dosed with the indicated Ni coverages and then with ~ 20 L of CO at 115 K.

K) [19]. Thus, a 3 ML Ni overlayer appears to show CO chemisorptive properties similar to a Ni(111) surface. The γ_2 state likely arises from the recombinative desorption of atomic O and C on the Mo(110) surface.

3.5. IR spectra of CO on Ni / Mo(110)

In this section, the IRAS spectra of CO adsorbed on Ni/Mo(110) will be presented and discussed. As will be seen, the ultra-thin Ni overlayers show quite different CO chemisorptive properties compared to a Ni(111) surface. In addition, the use of CO as a probe molecule allows the morphology and surface structures to be characterized by the analysis of the frequencies and line shapes of the CO IRAS peaks. In a previous study of CO adsorption on a Ni(111) surface using IRAS, it was reported that at 90 K, saturation CO (0.5 ML) predominantly occupies twofold bridging sites [20]. Furthermore, at elevated temperatures, a fast and reversible conversion between the bridge bound CO and linear CO was observed [20].

Figs. 5 and 6 show IRAS spectra of CO on Ni/Mo(110) at the indicated Ni coverages. For fig. 5, the Ni was deposited onto the Mo(110) surface at 90 K followed by exposure to 10 L of CO and spectral collection at 90 K. For fig. 6, the Ni overlayers were annealed to 900 K after Ni
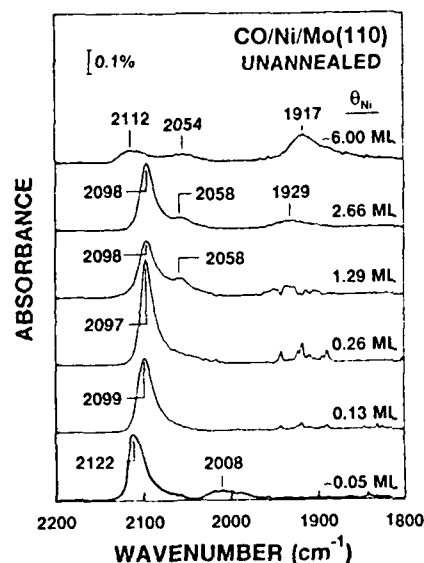
Fig. 5. IR spectra of CO on unannealed Ni/Mo(110) surfaces at the indicated Ni coverages. The Ni was deposited onto the Mo(110) surface at 90 K, dosed with 10 L of CO, followed by spectral acquisition at 90 K.
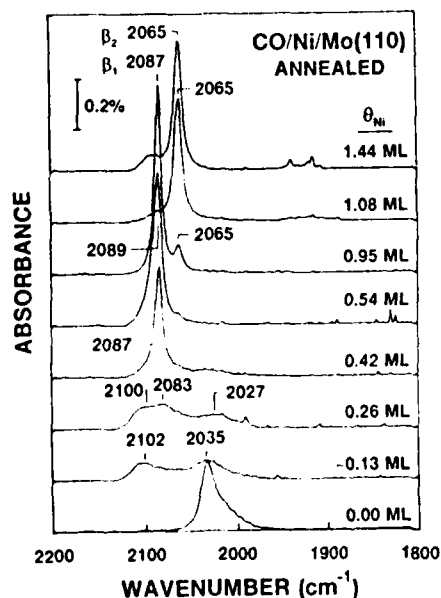

Fig. 7. Integrated intensity and frequency of the linear CO IR peaks in fig. 5 as a function of Ni coverage.

Fig. 6. IR spectra of CO on annealed Ni/Mo(110) surfaces at the indicated Ni coverages. Ni was deposited onto a Mo(110) surface at 90 K, annealed to 900 K, dosed with 10 L of CO, followed by spectral acquisition at 90 K.
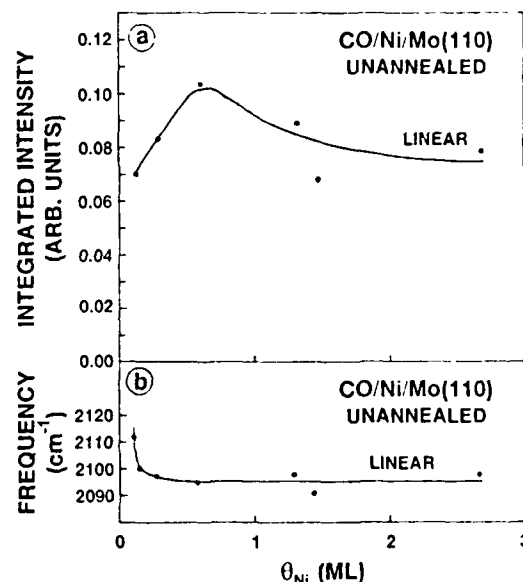
deposition and cooled to 90 K for CO exposure and spectral collection. The two main peaks at ~ 2100 and ~ 1920 cm^{-1} in fig. 5 are identified as linear and two-fold bridging CO, and the two main peaks at 2087 and 2065 cm^{-1} in fig. 6 are both identified as linear CO [20]. The integrated intensities and frequencies for the linear CO are plotted as a function of Ni coverage in figs. 7 and 8.

Several points in figs. 5–8 are noteworthy:

(1) For submonolayer Ni on Mo(110), the IRAS signal from CO on Mo is dramatically attenuated. On the unannealed Ni/Mo(110) surface, the intensity of CO–Mo is reduced to zero at a Ni coverage as low as 0.13 ML. On annealed Ni/Mo(110) surfaces, however, the CO–Mo peak at $\theta_{Ni} = 0.13$–0.26 ML shows considerable intensity, but has essentially disappeared by $\theta_{Ni} = 0.54$ ML. This strong attenuation of the CO–Mo peak by the submonolayer CO–Ni overlayer, is due to "intensity transfer" [21–23] and/or "screening" [23–26] effects. For "intensity transfer" there is a strong dipole–dipole coupling that transfers vibrational intensity from a low frequency mode to a high frequency mode [22]. This effect is most evident when the vibrational modes are separated
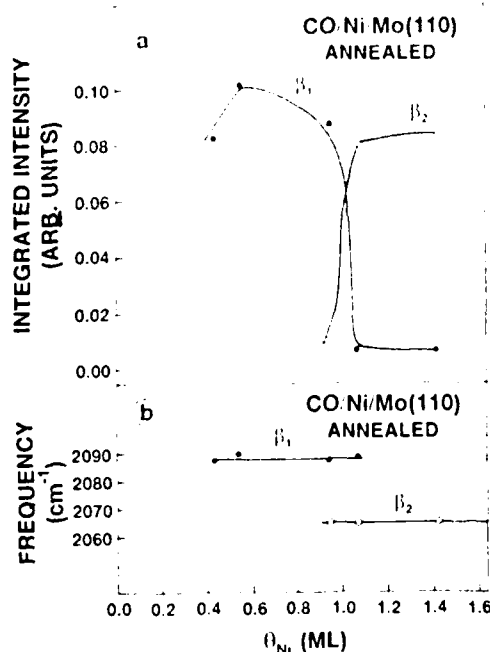
Fig. 8. Integrated intensity and frequency of the linear CO IR peaks in fig. 6 as a function of Ni coverage.

by less than a hundred wavenumbers as is seen in the spectra of co-adsorbed $^{12}C-^{16}O$ and $^{12}C-^{18}O$ where the observed IRAS peaks are at equal intensities for a 5% $^{12}C-^{16}O$/95% $^{12}C-^{18}O$ mixture [23]. In previous studies [24], a suppression in the IR intensity of a CO-Pt(111) peak has also been observed when CO is co-adsorbed with highly polarizable species (CH_3OH, H_2O, Xe). The polarizable species will induce a considerable shielding of the local electric field around the CO molecule, "screening" its dipole moment [24]. More importantly this effect has also been observed for CO adsorbed on submonolayer Cu and Ag on Pt(111) [25,26]. Due to the polarizability of the Cu and Ag adatoms upon CO adsorption, the CO-Cu and CO-Ag ensembles are effective at screening the CO-Pt [25,26]. For Ni/Mo(110), previous XPS studies have shown that submonolayer Ni films are quite polarizable, with the Ni($2P_{3/2}$) peak shifting ~0.6 eV upon CO adsorption [10]. In addition, fig. 6 shows that the CO-Ni and CO-Mo IR peaks are separated

by ~70 cm^{-1}. Together, these suggest that for Ni/Mo(110), "screening" will be more important than intensity transfer with regards to the attenuation of CO-Mo peak intensity. As mentioned earlier, the attenuation of the intensity of the CO-Mo peak is less for annealed Ni overlayers than for unannealed Ni overlayers. Upon annealing, the Ni overlayers form larger 2D Ni islands on the Mo(110) substrate and consequently more Ni atoms reside in the island interiors. Screening is less pronounced since a smaller function of the Mo surface is in close proximity to Ni adatoms. Thus, fig. 6 clearly shows that although the Ni coverage does not change during the annealing, "screening" is less pronounced for the annealed Ni overlayers allowing CO-Mo features to be visible up to Ni coverages of ~0.4 ML.

(2) For the first uniform Ni layer (θ_{Ni} = 1.29 ML), CO predominantly occupies linear sites. This is in contrast with the CO/Ni(111) system where nearly all CO molecules bind to two-fold bridge sites at 90 K [20]. The binding energy of the bridging CO on a Ni(111) surface was reported to be 0.3 kcal/mol higher than that of linear CO [20]. On the Ni(7×2) overlayer, linear CO is apparently more stable than bridging CO. As mentioned in section 3.3, the Ni(7×2) structure at θ_{Ni} = 1.29 ML assumes a distorted Ni(111) lattice. Previous work has also shown that the work function of the (7×2) structure is ~0.47 eV lower than that of a Ni(111) surface [9], and that the core level binding energies are shifted by 0.25 eV [10]. Therefore, the difference in the CO adsorption sites between the Ni(7×2) structure and a Ni(111) surface can be attributed to a combination of lattice strain and electronic perturbation in the Ni overlayers.

(3) Fig. 6 shows that the stretching frequency of CO on the (7×2) surface is 11 cm^{-1} lower than linear CO on Ni(111) (2054 cm^{-1}). For unannealed Ni multilayers (~6 ML), a peak at 2054 cm^{-1} is evident, and the bridging CO feature (1917 cm^{-1}) has considerable intensity. The high intensity of the bridging CO peak and the appearance of a peak at 2054 cm^{-1} strongly imply that the Ni is forming 3D clusters which have adsorption properties similar to those of a Ni(111) surface. The energy necessary for Ni to

diffuse and nucleate into 3D clusters could origi-
nate from its condensation energy. In a recent
paper, the diffusion and condensation energy of
Ag atoms on a W(110) surface were calculated to
be 3.5 and 50.7 kcal/mol, respectively [27]. A
fraction of the Ni condensation energy is, there-
fore, expected to be sufficient for Ni atoms to
migrate on the Mo(110) surface and to coalesce
into 3D clusters at these high coverages.

(4) On the annealed Ni/Mo(110) surfaces, the
linear CO peak shows an abrupt frequency shift
at 0.95 ML $< \theta_{Ni} <$ 1.1 ML (figs. 6 and 8). For
$\theta_{Ni} \leq$ 0.95 ML, the Ni/Mo(110) surface is charac-
terized by an (8 × 2) LEED pattern, while above
1.1 ML, a (7 × 2) pattern is observed. Therefore,
the abrupt frequency change in fig. 6 clearly
reflects the surface structural phase transition.
The (8 × 2) and (7 × 2) structures are character-
ized by CO IRAS peaks at 2087 and 2065 cm^{-1},
respectively [28]. As the Ni overlayers change
from the (8 × 2) to the (7 × 2) structure, the Ni
surface density increases 3% and the surface work
function increases by ~ 0.26 eV, approaching the
values for a Ni(111) surface [9]. The CO TPD
spectra (fig. 4) also show a 40 K increase in the
desorption temperature approaching the value
for CO on Ni(111). Correspondingly, during the
(8 × 2) to (7 × 2) phase transition, the CO
stretching frequency red shifts 22 cm^{-1} to ap-
proach that for linear CO on a Ni(111) surface.
Thus, we believe that the difference in the
stretching frequencies is due to the different elec-
tronic properties between the (8 × 2) phase and
the (7 × 2) phase. In addition, figs. 6 and 8 clearly
show that as the intensities of the 2087 and 2065
cm^{-1} peaks increase, the peak frequencies re-
main essentially unchanged, implying a 2D growth
mechanism in which the Ni islands grow via ex-
pansion at the island edges. The binding strength
and configuration of the CO at the interior of the
islands is virtually unaffected by island expansion.
A more detailed discussion on the use of IRAS
with CO as a probe molecule to study surface
structural phase transitions at metal–metal inter-
faces has been given elsewhere [28].

Fig. 9 shows the spectra for CO on 4.2 ML of
Ni on a Mo(110) surface as a function of CO
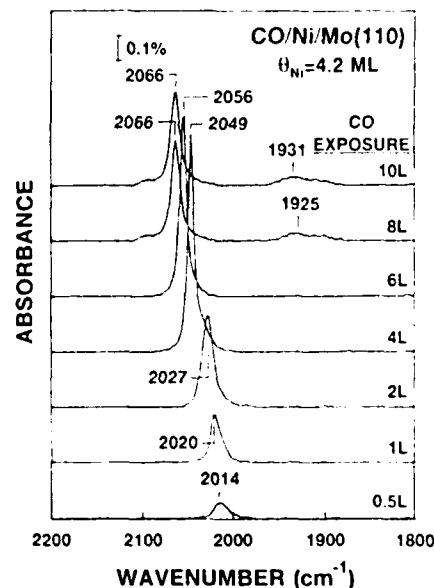exposure. The Ni/Mo(110) surface was annealed

Fig. 9. IR spectra of CO on 4.2 ML of Ni on a Mo(110)
surface as a function of CO exposure. The Ni was deposited
onto the Mo(110) surface at 90 K, annealed to 900 K, dosed
with the indicated CO exposures, followed by spectral collec-
tion at 90 K.

to 900 K prior to CO exposure and IR spectral
acquisition at 90 K. The integrated intensities,
full widths at half maximum and frequencies of
the IR peaks in fig. 9 are plotted in fig. 10 as a
function of CO exposure. As the CO exposure is
increased from 0.5 to 6 L, only linear CO is
evident. Bridging CO emerges at 8 L. This se-
quence is in direct contrast with the CO/Ni(111)
system where the bridging CO appears first, sug-
gesting that on the ultra-thin Ni films, linear CO
is energetically more stable than the bridging CO.
A frequency blue shift with an increase in CO
exposure is generally observed for CO/metal sys-
tems and is believed to be due to dipole–dipole
coupling and to electrostatic effects [21,22]. It is
noteworthy that as the CO coverage increases,
the linear CO intensity goes through a maximum
with a concurrent minimum in the FWHM, as
shown in fig. 10. This minimum can be attributed
to the formation of an ordered CO structure.
Order in the adsorbed CO molecules requires a
well ordered Ni overlayer. The ordering of the
CO molecules is further indicated by the highly

symmetric line shape of the IR spectra. It has been reported for CO/Ru(0001) that as the adsorbed CO forms an ordered structure, $(\sqrt{3} \times \sqrt{3})$-R30°, the corresponding FWHM showed a minimum, due to a reduction in the inhomogeneous broadening [29]. Thus, the decrease in the FWHM in figs. 9 and 10 indicates that the adsorbed CO is well ordered and that the order in the Ni overlayers is preserved during CO adsorption. This preservation of the order in the Ni overlayers is further confirmed by LEED results which show that the satellite spots of the (7 × 2) structure are present even following a 10 L CO exposure. Fig. 10 shows that the intensity of the linear CO peak decreases for CO exposures greater than 4 L. This could be due to depolarization [21] and/or the formation of bridging CO.

Fig. 11 shows the effect of annealing on the IR spectra of CO adsorbed on Ni/Mo(110). Ni was evaporated onto the Mo(110) surface at 90 K. The "a" and "u" indicate whether the sample
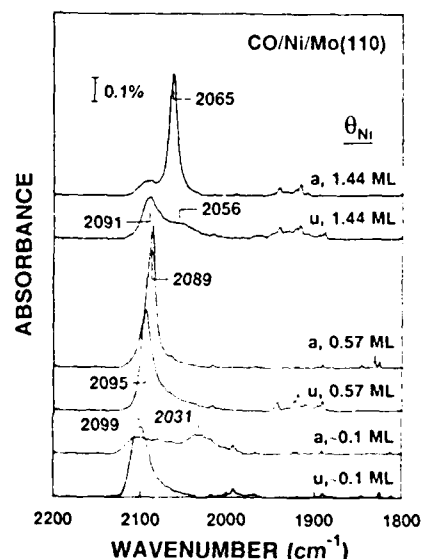

Fig. 11. IR spectra of CO on Ni/Mo(110) surfaces at the indicated Ni coverages. Ni was deposited onto a Mo(110) surface at 90 K, left unannealed (u) or annealed to 900 K (a), dosed with 10 L of CO, followed by spectral collection at 90 K.
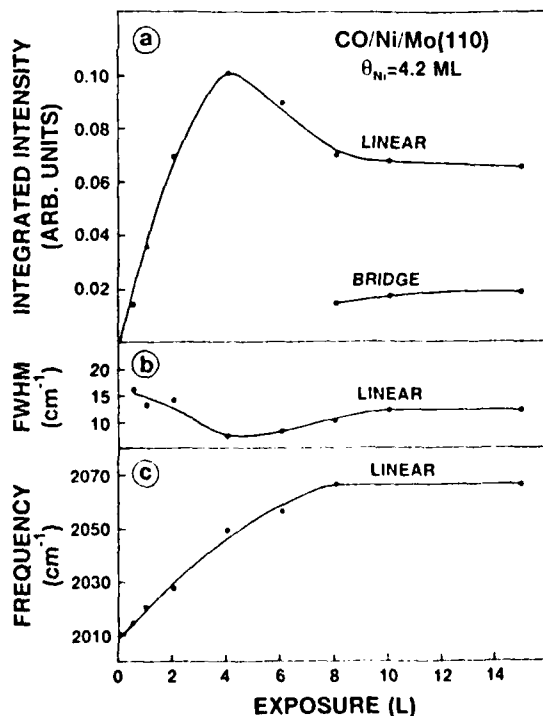

Fig. 10. Integrated intensity, full width at half maximum and frequency of the linear and bridge CO IR peaks in fig. 9 as a function of CO exposure.

was annealed to 900 K or left unannealed, respectively, after Ni deposition and before dosing 10 L of CO at 90 K. As shown in fig. 11, annealing 0.1 ML of Ni decreases the CO–Ni peak intensity with a concurrent increase in the CO–Mo peak intensity, indicating the formation of 2D Ni islands. As discussed above, as the size of the 2D islands increases, the "screening" effect is reduced leading to the increase in the CO–Mo peak intensity. At $\theta_{Ni} = 0.57$ ML, annealing yields a symmetric peak with a frequency red shift of 6 cm^{-1} compared to the unannealed surface. This change correlates with LEED results which indicate that at this coverage the Ni(8 × 2) structure forms from disordered Ni upon annealing. Annealing 1.44 ML of Ni/Mo(110) induces a new peak at 2065 cm^{-1} that is due to CO adsorbed onto the Ni(7 × 2) structure. It is also noteworthy that annealing decreases the bridging CO intensity, indicating that small 3D Ni clusters that formed during deposition have dispersed into 2D Ni islands.

In a previous study, it was shown that annealing a Cu/Rh(100) surface resulted in the forma-

tion of pseudomorphic Cu islands from disordered Cu atoms [11]. The ordered and disordered Cu islands could be characterized by two distinct CO IR peaks. Figs. 12 and 13 present data showing the formation of Ni(7 × 2) islands from disordered Ni. The spectra in fig. 12 were obtained by depositing 1.29 ML of Ni at 90 K, flashing to the indicated temperature, and then dosing with 10 L of CO at 90 K. Fig. 13 presents intensity and frequency plots as a function of annealing temperature for the spectra in fig. 12. As the Ni/Mo(110) surface is annealed above room temperature, the intensity of the peak at 2068 cm^{-1}, which corresponds to CO adsorbed on the Ni(7 × 2) structure, increases at the expense of the 2100 cm^{-1} peak that corresponds to CO adsorbed on disordered Ni islands. As in the Cu/Rh(100) system, disordered Ni and the ordered Ni(7 × 2) islands are unambiguously characterized by the two CO IR peaks (α and β). Fig. 13 indicates that up to an anneal temperature of ~ 900 K, the intensity of the two peaks changes nearly linearly, and the frequencies and total intensity remain essentially unchanged. The constant frequencies again imply a 2D growth mech-

Fig. 13. Integrated intensity and frequency of the linear CO IR peaks in fig. 12 as a function of annealing temperature.

anism with island expansion at the island edges. By using the integrated intensities to represent the Ni coverages in the disordered and the ordered islands, a van't Hoff plot can be obtained. This plot yields an enthalpy difference between the disordered and ordered Ni islands of 3.5 ± 0.4 kcal/mol. To deduce this enthalpy difference, it was assumed that the disordered and ordered phases were in equilibrium at the anneal temperature and that the phases transformed irreversibly upon annealing.

Figs. 14 and 15 show the temperature dependence of the IR spectra of CO on 1.29 and ~ 7 ML of Ni on Mo(110). The Ni was deposited at 90 K, flashed to 900 K, cooled to 90 K for a 10 L exposure of CO, and heated to the indicated temperatures for IR spectra collection. The intensities, frequencies and full widths at half maximum versus sample temperature are shown in figs. 16 and 17.

In fig. 14, the CO IR spectra show a peak at 2068 cm^{-1} that arises from CO adsorbed on the Ni(7 × 2) overlayer. For T_s > 220 K, CO begins desorbing with the CO peak frequency red shift-
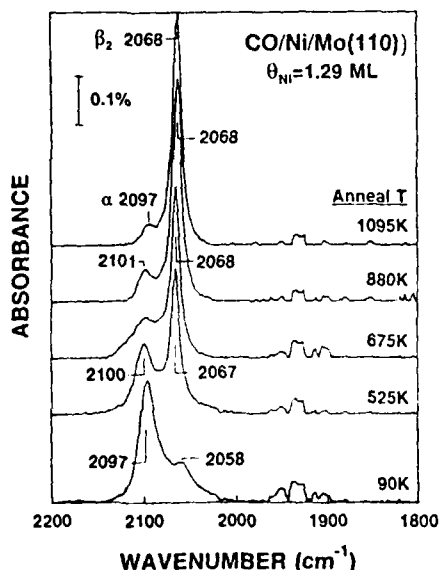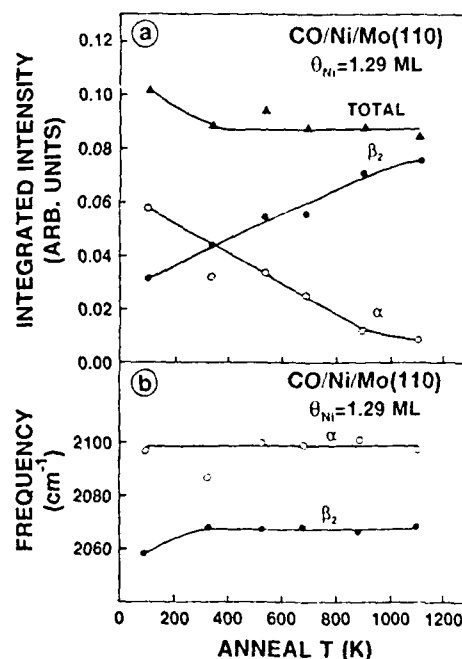

Fig. 12. IR spectra of CO on Ni/Mo(110) surfaces at a Ni coverage of 1.29 ML. The Ni was deposited onto the Mo(110) surface at 90 K, annealed to the indicated temperature, dosed with 10 L of CO at 90 K, followed by spectral collection.
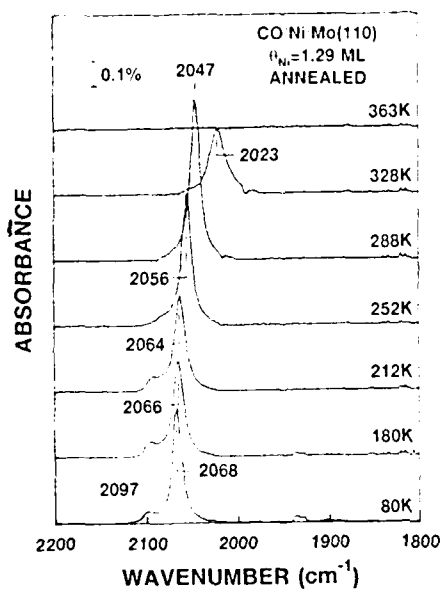
Fig. 14. IR spectra of CO on 1.29 ML of Ni on a Mo(110) surface. Ni was deposited onto the Mo(110) surface at 90 K, annealed to 900 K, and dosed with 10 L of CO at 80 K. The spectra were then acquired at the indicated temperatures.
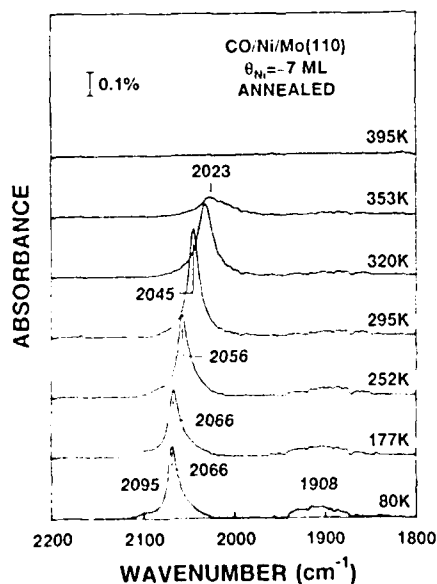
Fig. 16. Integrated intensity, full width at half maximum and frequency of the linear CO IR peak in fig. 14 as a function of sample temperature.

Fig. 15. IR spectra of CO on ~ 7 ML of Ni on a Mo(110) surface. Ni was deposited onto the Mo(110) surface at 90 K, annealed to 900 K, and dosed with 10 L of CO at 80 K. The spectra were then acquired at the indicated temperatures.
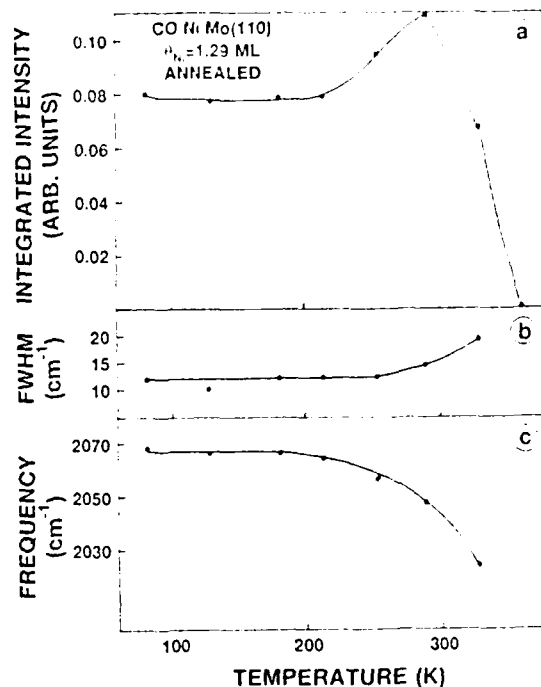
ing due to a reduction in dipole–dipole coupling. No CO conversion from linear to bridge sites is evident. Fig. 16 indicates a constant integrated intensity, FWHM and frequency at 90–200 K. As CO begins to desorb at $T_s > 220$ K, the integrated intensity increases and the frequency decreases due to the decrease in depolarization. In fig. 16, the FWHM also increases due to inhomogeneous broadening [21,22].

For CO on Ni multilayers (~ 7 ML), the spectrum at 80 K shows features from both linear and bridging CO (2066 and 1908 cm^{-1}, respectively). The TPD, LEED and AES results mentioned above indicate that the morphology of this surface is a uniform layer (the (7 × 2) structure) covered with 3D clusters having a slightly distorted Ni(111) lattice. The CO adsorbed onto the 3D clusters and onto the (7 × 2) layer apparently gives rise to the features at 1908 and 2066 cm^{-1}, respectively. Fig. 17 clearly shows that as the sample temperature is increased from 90 to 220 K, the intensity of the linear CO peak increases
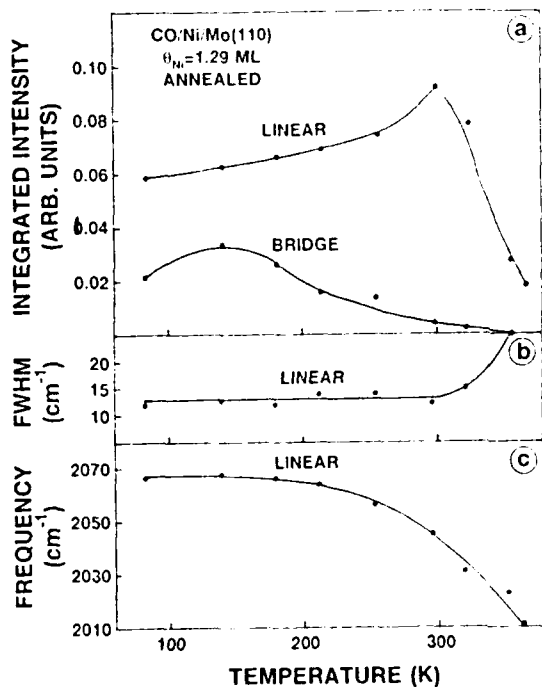
Fig. 17. Integrated intensity, full width at half maximum and frequency of the linear and bridging CO IR peaks in fig. 15 as a function of sample temperature.

Fig. 18. CO IR spectra obtained as follows: a Mo(110) surface was exposed to 10 L of CO at 80 K; ~0.1 ML of Ni was deposited onto the CO/Mo(110) surface at 80 K; the spectra were then collected at the indicated temperatures.

Mo(110) surface at 80 K, followed by heating to the indicated sample temperatures for IR spectral acquisition. The peak at ~ 2085 cm^{-1} for the

continuously, while the bridging CO intensity begins decreasing at $T_s > 140$ K. The conversion between linear and bridging CO on the 7 ML Ni overlayers is similar to CO on a Ni(111) surface [20], further demonstrating that the 7 ML Ni thin films resemble a Ni(111) surface with respect to CO adsorption.

In several recent studies, metal overlayers have been deposited onto CO precovered metal surfaces [30–33]. It has been reported for Cu deposition onto CO/Ru(0001) and Co/W(110) that the complex structures Cu/CO/Ru(0001) [30] and Cu/CO/W(110) [31] are formed at ~ 90 K. The deposition of Pd onto CO/W(110) and Cu onto CO/Rh(100), however, were reported to generate the more conventional structures CO/Pd/W(110) [32] and CO/Cu/Rh(100) [33] due to CO diffusion from the substrate surface onto the metal overlayers. Figs. 18 and 19 present the CO IR spectra that were obtained from Ni deposition (~ 0.1 and 1.6 ML) onto a CO precovered
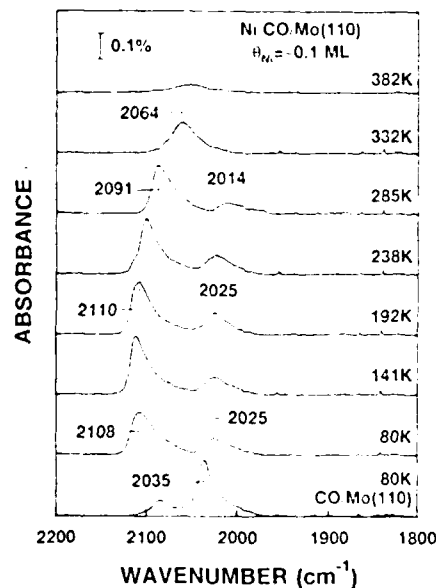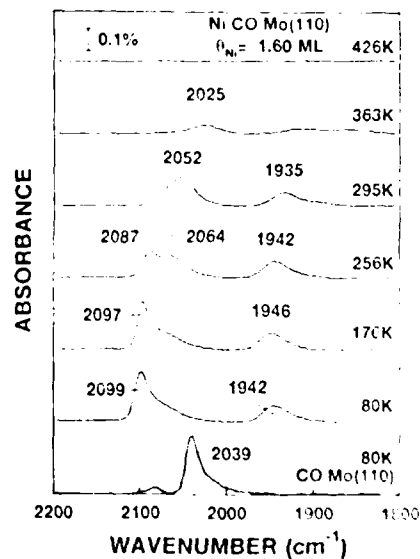

Fig. 19. CO IR spectra obtained as follows: a Mo(110) surface was exposed to 10 L of CO at 80 K; 1.60 ML of Ni was deposited onto the CO/Mo(110) surface at 80 K; the spectra were then collected at the indicated temperatures.

CO/Mo(110) spectrum in each figure is due to low-level C contamination.

It is clear from figs. 18 and 19 that the deposition of Ni at 80 K induces a new peak at ~ 2100 cm^{-1}. This peak is due to CO adsorbed onto Ni and indicates that CO has diffused onto the Ni overlayers. The peaks at ~ 2025 (fig. 18) and 1940 cm^{-1} (fig. 19) arise from CO adsorbed onto the Mo substrate and from bridging CO on 3D Ni clusters, respectively. The asymmetric peak shapes for the 80 K spectra indicate that the Ni atoms are disordered. As the sample temperature is increased, the intensities of CO–Ni and CO–Mo remain essentially unchanged, indicating that the spill-over of CO from Mo to Ni at 80 K is complete. This also indicates negligible diffusion of CO between Ni and Mo sites. In fig. 19, heating the surface to 256 K induces a new peak at 2064 cm^{-1} that corresponds to CO adsorbed onto a Ni(7 × 2) overlayer. The invariant bridging CO intensity indicates that there is little transfer of CO from the bridged to the linear sites. The binding energies of Ni and CO on a Mo(110) surface are 92 and 23 kcal/mol, respectively (see sections 3.2 and 3.4). This difference (69 kcal/mol) apparently serves as the driving force for the CO migration.

(3) Two LEED structures ((8 × 2) and (7 × 2)) are observed for Ni/Mo(110) surfaces. These two structures are interpreted to be distorted Ni(111) lattices. The (8 × 2) structure is found to transform into the (7 × 2) structure at a Ni coverage between 0.95 and 1.29 ML.

(4) TPD spectra of CO from the first uniform layer of Ni on a Mo(110) surface show desorption peaks with activation energies lower than those from a Ni(111) surface, due to an electronic perturbation of the Ni overlayer by the substrate.

(5) For submonolayer Ni on a Mo(110) surface, CO predominantly occupies linear sites. Bridging CO is mainly found on 3D Ni clusters that have a distorted Ni(111) structure.

(6) On an annealed Ni/Mo(110) surface, the (8 × 2) to (7 × 2) structural phase transition is clearly reflected in the CO IR spectra. The two structures are characterized by CO stretching frequencies at 2087 and 2065 cm^{-1}, respectively. Furthermore, the formation of ordered (7 × 2) islands from disordered Ni upon annealing is also indicated in the CO IR spectra.

(7) The deposition of Ni onto a CO presaturated Mo(110) surface at $T_s = 80$ K causes CO to spill-over from the Mo surface to the Ni overlayer, and thus leads to a CO/Ni/Mo(110) structure.

4. Summary

In this paper, we have reported and discussed the experimental results for ultra-thin Ni films supported on a Mo(110) surface in terms of film morphology, structures, surface phase transitions, CO adsorption and CO surface diffusion. The main conclusions are summarized as follows:

(1) The AES results show that Ni grows on a Mo(110) surface layer by layer at $T_s = 115$ K. Upon annealing, Ni multilayers form 3D clusters at $T_s > 600$ K.

(2) Two peaks (β_1 and β_2) are observed in the desorption spectra of Ni from Mo(110) and correspond to desorption of 3D Ni clusters and the first uniform layer, respectively. The desorption of the 3D clusters follows zero order kinetics with an activation energy of 91.9 kcal/mol.

Acknowledgments

References

[1] J.A. Rodriguez, R.A. Campbell and D.W. Goodman, J. Phys. Chem. 95 (1991) 4196.

[2] (a) P.J. Berlowitz and D.W. Goodman, Surf. Sci. 187 (1987) 463.
(b) J. Kolaczkjenicz and E. Bauer, Surf. Sci. 144 (1984) 495.

[3] P.J. Berlowitz and D.W. Goodman, Langmuir 4 (1988) 1091.

[4] B.G. Johnson, P.J. Berlowitz, D.W. Goodman and C.H. Bartholomew, Surf. Sci. 217 (1989) 13.

[5] P.J. Berlowitz, J.-W. He and D.W. Goodman, Surf. Sci. 231 (1990) 315.

[6] D.W. Goodman and C.E.F. Peden, J. Chem. Soc. Faraday Trans. I 83 (1987) 1967.

[7] P.J. Berlowitz, J.E. Houston, J.M. White and D.W. Goodman, Surf. Sci. 205 (1988) 1.

[8] C.T. Campbell and D.W. Goodman, J. Phys. Chem. 92 (1988) 2569.

[9] M. Tikov and E. Bauer, Surf. Sci. 232 (1990) 73.

[10] R.A. Campbell, J.A. Rodriguez and D.W. Goodman, Surf. Sci. 256 (1991) 272.

[11] J.-W. He, W.K. Kuhn, L.-W.H. Leung and D.W. Goodman, J. Chem. Phys. 93 (1990) 7463.

[12] B.C. Gates, J.R. Katzer and G.C.A. Schuit, Chemistry of Catalytic Process (McGraw-Hill, New York, 1979).

[13] D.W. Goodman, J.T. Yates, Jr. and C.H.F. Peden, Surf. Sci. 164 (1985) 417.

[14] L.-W.H. Leung, J.-W. He and D.W. Goodman, J. Chem. Phys. 93 (1990) 8328.

[15] M. Grunze, H. Ruppender and O. Elshazly, J. Vac. Sci. Technol. A 6 (1988) 1266.

[16] Lange's Handbook of Chemistry, 13th ed. (McGraw-Hill, New York, 1985) pp. 9–124.

[17] (a) E. Bauer, Surf. Sci. 7 (1967) 351.
(b) N.J. Taylor, Surf. Sci. 4 (1966) 161.

[18] P.A. Redhead, Vacuum 12 (1962) 203.

[19] K. Christmann, O. Schober and G. Ertl, J. Chem. Phys. 60 (1974) 4719.

[20] Th. Surnev, Z. Xu and J.T. Yates, Jr., Surf. Sci. 201 (1988) 14.

[21] F.M. Hoffmann, Surf. Sci. Rep. 3 (1983) 107.

[22] R. Ryberg, in: Advances in Chem. Phys., Ed. K.P. Lawley (Wiley, New York, 1989) p. 1.

[23] B.N.J. Persson and R. Ryberg, Phys. Rev. B 24 (1981) 6954.

[24] D.H. Ehlers, A.P. Esser, A. Spitzer and H. Luth, Surf. Sci. 191 (1987) 466.

[25] J.A. Rodriguez, C.M. Truong and D.W. Goodman, J. Chem. Phys., in press.

[26] J.A. Rodriguez, C.M. Truong and D.W. Goodman, Surf. Sci., in press.

[27] G.W. Jones, J.M. Marcano, J.K. Norskov and J.A. Venables, Phys. Rev. Lett. 65 (1990) 3317.

[28] (a) J.-W. He, W.K. Kuhn and D.W. Goodman, J. Am. Chem. Soc. 113 (1991) 6416.
(b) W.K. Kuhn, J.-W. He and D.W. Goodman, J. Vac. Sci. Technol. A 10 (1992), in press.

[29] H. Pfnur, D. Menzel, F.M. Hoffmann, A. Ortega and A.M. Bradshow, Surf. Sci. 93 (1980) 431.

[30] F.M. Hoffmann, G. Rocker, H. Tochihara, R.M. Martin and H. Metiu, Surf. Sci. 205 (1988) 397.

[31] N. Shamir, J.C. Lin and R. Gomer, J. Chem. Phys. 90 (1989) 5135.

[32] J.C. Lin, N. Shamir and R. Gomer, Surf. Sci. 226 (1990) 26.

[33] J.-W. He, W.K. Kuhn and D.W. Goodman, J. Phys. Chem. 95 (1991) 5220.